

ICSV14

Cairns • Australia
9-12 July, 2007



NOISE PREDICTION OF A SERRATED NOZZLE USING A HYBRID APPROACH

Dandy Eschricht, Lukasz Panek, Jianping Yan, Frank Thiele^{1*}, Marc Jacob²

¹Institute for Fluid Mechanics and Engineering Acoustics (ISTA)
Berlin University of Technology
10623 Berlin, Germany

²Ecole de Centrale de Lyon
Lyon, France
eschricht@cfdf.tu-berlin.de

Abstract

In this work simulation and far-field sound prediction results are presented for a number of subsonic, coaxial jet flow configurations of high Reynolds number. Two casing geometries have been examined, and in both cases the nozzle lip of the outer nozzle was studied with and without serrations. The unsteady Reynolds-Averaged-Navier-Stokes Equations have been solved using a finite volume solver. A modified version of the Detached Eddy Simulation (DES) has been applied to model unresolved turbulence. The DES is based on a two equation turbulence model with a modified length scale definition. Far-field acoustic results were obtained using the acoustic analogy of Ffowcs-Williams & Hawkings. The predicted overall sound pressure levels agree well with measurements, while deviations are within a 3dB range, meaning that the dominant noise sources have been captured in the simulation on relatively coarse grids.

1. INTRODUCTION

Acoustic emissions from jet engine exhausts now constitute a major noise source during take-off. Additionally, with recent successes in the attenuation of other noise sources, jet exhausts during take-off are a central focus in the overall scheme of noise reduction in airplanes. Significant advancements have already been seen, for instance high bypass ratios and modification of the nozzle geometry adding tabs or serrations.

Numerical simulation of the flow field allows an in-depth analysis of the flow phenomena involved and the mechanisms of noise generation. In this work, simulation results for high subsonic coaxial jet flows are presented for two configurations. Both configurations are typical jet exhausts that have both been studied with a plane nozzle and with passive flow control (serrated) on the nozzle lip. They are investigated using far-field sound characteristics obtained by the Ffowcs-Williams-Hawkings acoustic analogy [1][2] and compared to experimental measurements. An analysis of the flow field is subsequently carried out comparing the configurations.

The flow fields of the smooth and serrated nozzles have been simulated using Detached Eddy Simulation (DES). This strategy employs a turbulence model consistently blending between Reynolds-Averaged Navier-Stokes (RANS) and Large Eddy Simulation (LES) approaches. As compared with a fully resolved LES including the inner nozzle flow, the DES allows for coarser grids, esp. in the near wall region, while preserving the wall boundary layer characteristics. It is well-known that in order to obtain high quality sound prediction, accurate reproduction of the wall boundary layer, and thus of the nozzle exit profiles, is essential. To facilitate comparisons, the inner nozzle flow is therefore included in all configurations. Consequently, the implicit dependence of the sound field on the otherwise required boundary specifications at the nozzle exit and forcing parameters could be avoided. In general, this work aims at summarising the results obtained by our group applying the DES for jet flow simulations.

2. GOVERNING EQUATIONS

The equations solved are the Reynolds-averaged continuity, momentum and energy equations:

$$\frac{\partial \rho}{\partial t} + \frac{\partial(\rho u_i)}{\partial x_i} = 0, \quad (1)$$

$$\frac{\partial(\rho u_i)}{\partial t} + \frac{\partial(\rho u_i u_j)}{\partial x_j} = -\frac{\partial p}{\partial x_i} + \frac{\partial \sigma_{ij}}{\partial x_j} + \frac{\partial \tau_{ij}}{\partial x_j}, \quad (2)$$

$$C_p \left[\frac{\partial(\rho T)}{\partial t} + \frac{\partial(\rho u_i T)}{\partial x_i} \right] = \frac{\partial p}{\partial t} + u_i \frac{\partial p}{\partial x_i} - \frac{\partial \dot{q}_i}{\partial x_i} + \tau_{ij} \frac{\partial u_j}{\partial x_i}, \quad (3)$$

where σ_{ij} and τ_{ij} are the viscous stress tensor and the modeled Reynolds stress tensor, respectively. They are defined as

$$\sigma_{ij} = 2\mu(S_{ij} - \frac{1}{3}S_{kk}\delta_{ij}), \quad (4)$$

$$\tau_{ij} = 2\mu_t(S_{ij} - \frac{1}{3}S_{kk}\delta_{ij}) - \frac{2}{3}\rho k \delta_{ij}, \quad (5)$$

hereby S_{ij} denotes the strain rate tensor which reads $S_{ij} = \frac{1}{2}(\frac{\partial u_i}{\partial x_j} + \frac{\partial u_j}{\partial x_i})$, while μ_t is the turbulent dynamic viscosity. The heat flux appearing in the energy equation is modeled using a temperature gradient approach:

$$q_j = C_p \left(\frac{\mu_t}{Pr_t} + \frac{\mu}{Pr} \right) \frac{\partial T}{\partial x_j}, \quad Pr_t = 0.9. \quad (6)$$

2.1. Turbulence Modeling

The unresolved turbulent quantities are modeled by the Wilcox $k - \omega$ model defined as

$$\frac{\partial \rho k}{\partial t} + \frac{\partial(\rho u_j k)}{\partial x_j} = \frac{\partial}{\partial x_j} \left[\left(\mu + \frac{\mu_t}{\sigma_k} \right) \frac{\partial k}{\partial x_j} \right] + \rho P_k - C_\mu \rho k \omega, \quad (7)$$

$$\frac{\partial \rho \omega}{\partial t} + \frac{\partial(\rho u_j \omega)}{\partial x_j} = \frac{\partial}{\partial x_j} \left[\left(\mu + \frac{\mu_t}{\sigma_\omega} \right) \frac{\partial \omega}{\partial x_j} \right] + C_{\omega 1} \frac{\omega}{k} \rho P_k - C_{\omega 2} \rho \omega^2, \quad (8)$$

with the turbulent viscosity $\mu_t = \rho \frac{k}{\omega}$, the production term $P_k = \nu_t S^{*2}$, $S^* = \sqrt{2S_{ij}S_{ij}}$. The model constants are determined as

$$C_\mu = 0.09, \quad c_{\omega 1} = 5/9, \quad c_{\omega 2} = 3/40, \quad \sigma_k = \sigma_\omega = 2.0.$$

Equations 7 and the expression for the turbulent viscosity are rewritten introducing a length scale to allow the DES modifications

$$\frac{\partial \rho k}{\partial t} + \frac{\partial(\rho u_j k)}{\partial x_j} = \frac{\partial}{\partial x_j} \left[\left(\mu + \frac{\mu_t}{\sigma_k} \right) \frac{\partial k}{\partial x_j} \right] + \rho P_k - \frac{\rho k^{3/2}}{L}, \quad (9)$$

$$\mu_t = \rho C_\mu L \sqrt{k}. \quad (10)$$

where L denotes the modeled length scale. In order to reduce the “grey area problem” described below, eq. 10 represents a DES modification proposed by *Yan et al* [3] that also affects the production term. For the RANS region, the length scale is consistently defined as

$$L = L_{RANS} = \frac{\sqrt{k}}{C_\mu \omega}, \quad (11)$$

while for the LES-mode region it is estimated from the local grid spacing Δ . For the simulations presented, the following definition is used

$$L = L_{DES} = \min(L_{RANS}, C_{DES} \Delta), \text{ with } \Delta = (\Delta_x \Delta_y \Delta_z)^{1/3} \quad (12)$$

where Δ_x , Δ_y and Δ_z represent the local, spatial dimensions of the cell. This definition allows consistent blending between an unresolved RANS region ($C_{DES} \Delta > L_{RANS}$) and a resolved LES region ($C_{DES} \Delta < L_{RANS}$).

The definition of Δ differs from the more common $\Delta = \max(\Delta_x, \Delta_y, \Delta_z)$. In fact, the difference is small for near cubic cells, but increases for cells of large aspect ratio. The definition used here, aims at overcoming the effects of the so called “grey area” problem in DES, that occurs between the RANS and fully resolved LES region, when the model switches to LES mode but no resolved turbulence is contained in the flow field. Further, high modeled turbulent kinetic energy and viscosity are convected into the “grey area”, that further damps the development of turbulent perturbations.

Concerning jet flow simulations these problems occur at the nozzle lip where the unresolved wall boundary layer becomes a free shear layer. In a too viscous flow the natural instability of the shear layer is suppressed and transition to resolved turbulence delayed. The problem is not unique to DES. While doing a LES of coaxial jet, *Andersson et al* [4] could enhance simulation results when using the cubic root length scale definition. It can be argued that the use of cubic root length scale definition does not reflect the grid resolution properties correctly, but as the simulation results are enhanced by it, one can conclude that no serious violation of the turbulent flow properties is created. Some additional comparison of different modeling approaches in DES for jet flows can be found in *Yan et al* [6] and a more detailed description of the simulation method in *Yan et al* [7].

3. CONFIGURATIONS AND CONDITIONS

Both simulated nozzles operate under realistic conditions with a heated primary stream. The nozzle geometries and flow conditions are equal between the serrated and plane nozzle lip, except for the 20 serrations that are added to the plane lip in both cases. The added serrations are aligned with flow direction for the short cowl nozzle, while pointing into the flow at an angle of 7 degrees for the long cowl nozzle. Further details on the two configurations is given below.

3.1. Short cowl nozzle

The short cowl nozzle operates under the following conditions: primary stream exit Mach number $Ma_p = 0.861$, secondary stream exit Mach number $Ma_s = 0.902$, ambient flow Mach number $Ma_{amb} = 0.03$, a temperature ratio between primary stream and the ambient of $R_p = 2.7$ and a temperature ratio between secondary stream and the ambient of $R_s = 1$. The grid for plane lip configuration resolves the azimuthal direction with 60 cells, while 160 cells are used for the serrated case. This leads to about 4 million cells for the plane, and to 11 million cells for the serrated configuration.

3.2. Long cowl nozzle

The second configuration, the long cowl nozzle, operates under the following conditions: primary stream exit Mach number $Ma_p = 0.44$, secondary stream exit Mach number $Ma_s = 0.6$, ambient flow Mach number $Ma_{amb} = 0.26$, the temperature ratio $R_p = 2.68$ and $R_s = 1.125$. These conditions lead to Mach numbers between 0.6 and 0.8 at the exit plane of the casing. Each serration is resolved with 16 cells in circumferential direction, leading to 320 circumferential cells for the whole mesh, while 120 cells have been used for the plane case. This amounts to a total number of 26 and 9 million cells for the serrated and the plane case, respectively.

The majority of grid points is concentrated in the near nozzle region, especially in the shear layers. In the radial direction the grid coarsens fast for positions $r > 1/2D_s$ which is expected have some effect on the propagation of acoustic wave of smaller wave lengths to the FWH-surface. In the axial direction the grid coarsens for positions $x > 5D$. This affects the capturing of sources beyond the potential core.

For all configurations the time step size used in the simulations is based on the convective time unit \mathcal{T} which is defined as $\mathcal{T} = D_s/U_s$, based on the outer diameter D_s of the nozzle and the exit velocity of the secondary stream U_s . A time step size of $\Delta t = \mathcal{T}/360$ has been used, thus corresponding to a Strouhal frequency $St = fD_s/U_s$ of about 360.

4. RESULTS

4.1. Flow field

Flow field results are shown in terms of instantaneous isosurfaces for the configurations in figures 2 and 3 visualising the behaviour of the shear layers. Concerning the short cowl configuration, the effect of the serrations is only slightly visible at the outer shear layer, and they seem only to affect the flow close to nozzle lip. The effect is more enhanced at the inner shear layer, as the structures in the outer shear layer affect the inner at an earlier stage. This conclusion can be drawn from the stronger fluctuations appearing at a more upstream position compared to the

plane configuration in figure 2.

As the serrations point into the flow for the long cowl nozzle, their effect is much stronger. The isosurfaces of the λ_2 -criterion (Jeong *et al* [5]) show ring-like structures in the shear layer close to the nozzle lip for the plane configuration. The serrations force transition to turbulence directly at the nozzle lip, here visible by much stronger vortical structures in the initial shear layer that are much smaller in size.

4.2. Far field acoustics

The far field prediction has been obtained by an acoustic analogy by Ffowcs-William & Hawkings. During the simulation flow field data was stored for a surface surrounding the jet that are depicted for the short cowl configuration in figure 5 by the black line. The obtained far field acoustic results are depicted in figure 4, comparing the overall sound pressure level (OASPL) for different angles to the jet axis with measurements. The far field predictions show a good agreement with the measurements.

The maximum deviations of about 3dB occur around angles of 45° for the short cowl nozzle and at around 70° for the long cowl configuration. These deviations are attributed to the grid resolution in the axial direction which coarsens fast downstream of the potential core. Therefore, sources in this region are not well captured. Visual evidence of this can be found in figure 5 showing instantaneous contours of the z-vorticity in the xy-plane from the plane lip, short cowl nozzle simulation. Downstream of $x = 5D_s$ the structures show a fast decay in magnitude until they nearly disappear at larger axial positions.

Comparing the plane and serrated short cowl nozzle, the experiment predicts a noise reduction of about 2dB for all angles. The numerical noise prediction is able to follow this trend, while the deviations remain at the a similar order of magnitude.

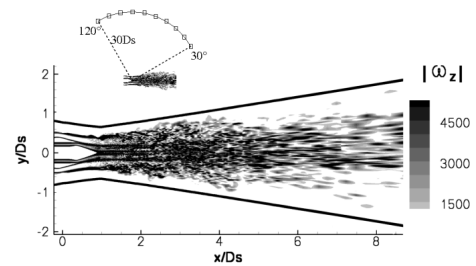


Figure 5. Z-vorticity and slice through the FWH-surface for the short cowl nozzle

5. SUMMARY AND CONCLUSION

Detached Eddy Simulations of a number of turbulent, heated jets have been carried out with the aim to provide data for an acoustic far field prediction by an acoustic analogy (FWH). The DES was modified to account for the flow physics of the jet flow. The plane and serrated nozzle geometries were directly included in the simulation. No artificial forcing was done during the simulation. The simulated flow fields show the effects of the serrated geometries and of the coarsening grids. Some evidence of enhanced turbulent mixing was found in the simulation that has to be further examined in terms of flow field statistics of turbulent quantities and average flow properties.

Although the flow field is affected by the grids being too coarse in certain regions, the acoustic predictions agree well with the measurements. The deviations found are within a 3dB level and can be attributed to the grid coarsening that leads to a lack of sources downstream of the potential core. The effect of the serrations on the acoustic field is reproduced by the

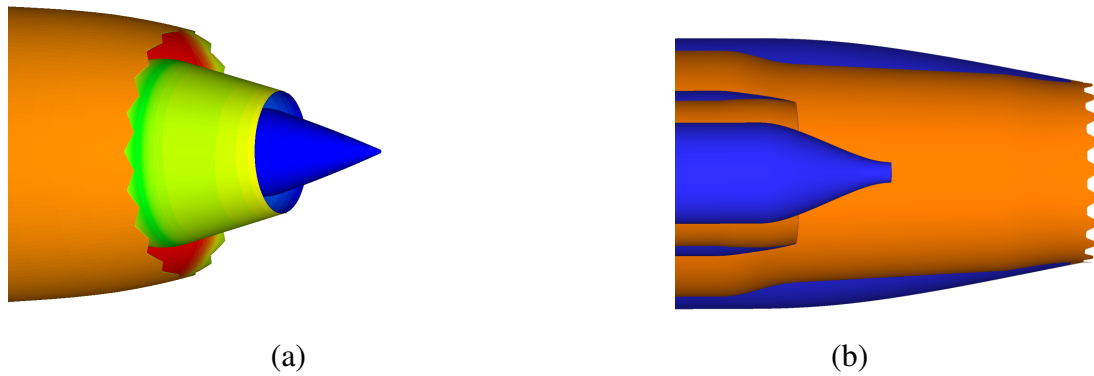


Figure 1. Geometries of the short cowl configuration (a), and the long cowl configuration (b)

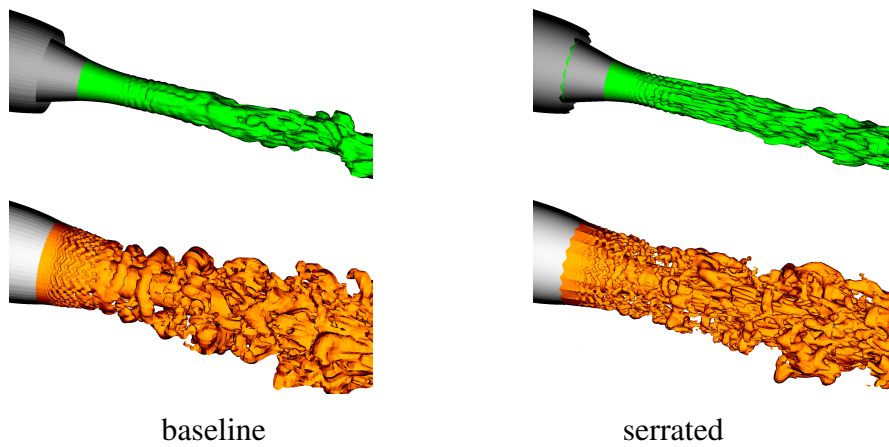


Figure 2. Instantaneous isosurfaces of density showing the flow structures in the shear layers for the short cowl configuration; Bottom: between the primary and secondary stream ($\rho = 0.90\text{kg}/\text{m}^3$); Top: between the secondary stream and surrounding flow ($\rho = 1.19\text{kg}/\text{m}^3$)

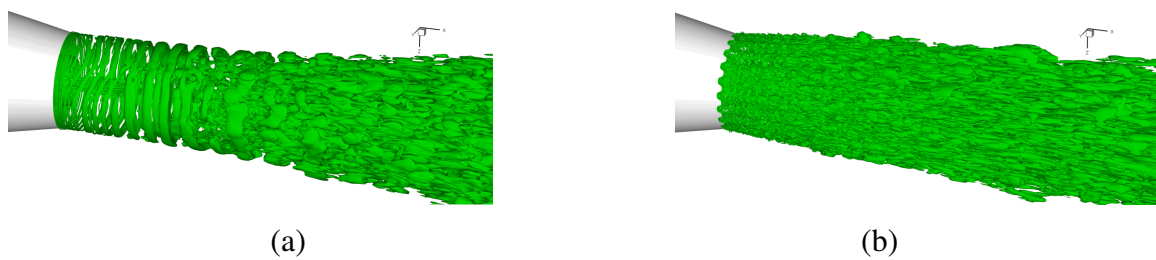


Figure 3. Instantaneous isosurfaces of λ_2 criterion; plane lip (a), serrated lip (b)

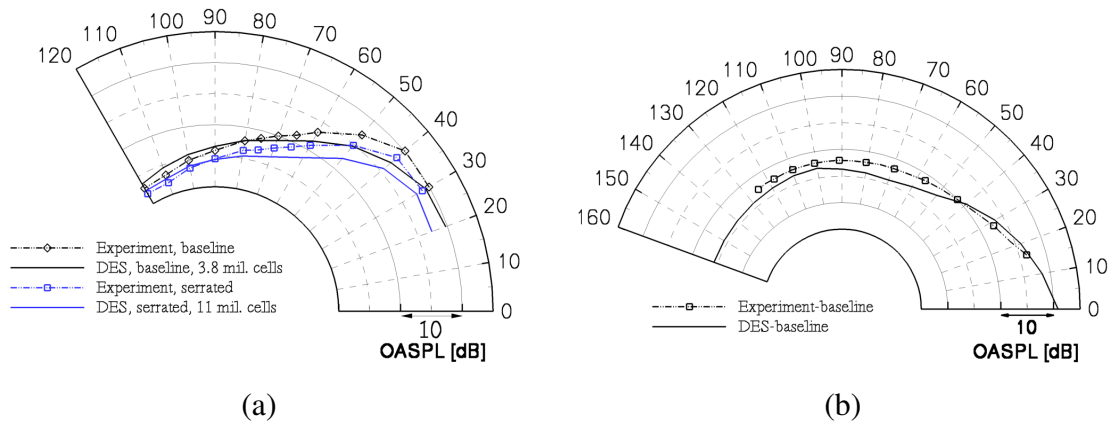


Figure 4. Overall sound pressure level of DES/FWH approach compared to measurements; short cowl nozzle (a), long cowl nozzle (b)

joined DES/FWH method that is also able to predict the trend of a general sound reduction. The deviations in the acoustic prediction remain on the same error level.

The obtained results show that the applied simulation and sound prediction methods are capable of reproducing the jet flow physics and the acoustic far field. A further enhancement of the results can be achieved by a better grid resolution in the region downstream of the potential core.

REFERENCES

- [1] J. Ffowcs-Williams and D. Hawkings, "Sound generation by turbulence and surfaces in arbitrary motion", *Phil. Trans. Roy. Soc.* **264**:321-342, 1969
- [2] F. Farassat, "Theory of Noise Generation from Moving Bodies with Application to Helicopter Rotors", *NASA Technical Report*, TR-451, 1975
- [3] J. Yan, C. Mockett and F. Thiele, "Investigation of Alternative Length Scale Substitutions in Detached-Eddy Simulation", *Flow Turbulence and Combustion*, **74**:85-102, 2005
- [4] N. Andersson, L.E. Eriksson and L. Davidson, "LES prediction of flow and acoustic field of a coaxial jet", *AIAA Paper 2005-2884*, 11th AIAA/CEAS Aeroacoustics Conference, 2005
- [5] J. Jeong and F. Hussain, "On the identification of a vortex", *J. Fluid Mech.*, **285**:69-94, 1995
- [6] J. Yan, D. Eschricht, F. Thiele and X. Li, "Modeling and Simulation of Coaxial Jet Flow", *Proceedings of the Fifth International Conference on Fluid Mechanics*, August 15-19, Shanghai, China, 2007
- [7] J. Yan, K. Tawackolian, U. Michel and F. Thiele, "Computation of Jet Noise using a Hybrid Approach", *AIAA Paper 2007-3621*, 13th AIAA/CEAS Aeroacoustics Conference, 2007